06

Mathematical modeling of the process of cold sintering of ceramics under pressure

© E.V. Radkevich,[1] A.V. Ragutkin,[2,3] M.E. Stavrovsky,[4] M.I. Sidorov,[3] O.A. Vasilyeva,[5] I.N. Kravchenko[2]

[1]Moscow State University,
Moscow, Russia
[2]Blagonravov Institute of Machine Science, Russian Academy of Sciences,
Moscow, Russia
[3]MIREA - Russian Technological University,
Moscow, Russia
[4]Bauman Moscow State Technical University,
Moscow, Russia
[5]Moscow State University of Civil Engineering,
Moscow, Russia
e-mail: kravchenko-in71@yandex.ru

Received September 6, 2025
Revised October 4, 2025
Accepted October 7, 2025

The article is devoted to mathematical modeling of the process of cold sintering under pressure. A theoretical analysis of cold sintering mechanisms is presented. The quantitative description of the cold pressure sintering process is described by a number of accompanying and dynamic phenomena. A mathematical model of cold sintering of ceramics under pressure is proposed, which allows predicting the approach of the process to a local equilibrium that determines the mechanisms of consolidation, grain growth and formation of defects in the structure.

Keywords: modeling, cold pressure sintering, ceramics, phase transition, diffusion, crystallization, consolidation.

DOI: 10.61011/TP.2026.03.63165.255-25

Introduction

Cold sintering process (CSP) is a relatively new low-temperature technique for densifying ceramic materials [1–3]. Besides the obvious benefits in terms of energy consumption, CSP enables production of unique materials and composites. Potential integration of ceramics with organic materials [4,5] provides a new class of hybrid components. Since the first Guo's report [2], CSP has gained great interest among researchers of semiconductor materials [6], ionic conductors [7–10], piezoelectric ceramics [11], ferroelectric materials [12], Li-ion battery materials [13], nanocomposite materials [14] and low-loss ceramics [15].

Despite a large body of literature concerning cold sintering of ceramics [16,17], analytical study of the densification and grain growth phenomenon is not available yet. Theoretical analysis of mechanisms acting during the cold sintering process is described in [1]. The analysis is focused on two cold sintering approaches characterized by using either isostatic or uniaxial pressure. CSP is a technique for sintering in liquid phase under pressure where the transient liquid phase generally contains water [3]. Interaction between water and material plays a key role by facilitating formation of surface defects and secondary phases. Densification takes place at a temperature ranging from room temperature to 200 °C, above the boiling point. Compaction is considered to be caused by the dissolution and redeposition process, which can be associated with Ostwald ripening and recrystallization. There are two known types of dissolution in ceramics: congruent and incongruent. Congruent dissolution is the process where the composition of a solid body remains unchanged because the dissolved material has the same stoichiometry as the initial phase. In CSP, congruent dissolution occurs *in-situ* by powder compaction in liquid medium. CSP is similar to lithification of rock in high pressure conditions in liquid [10], and resembles biomineralization in sea sponges or organisms [18].

1. Model selection

Taking into account all full-scale experiment data, it is more reasonable for the mathematical simulation of cold sintering to use an approach employed for the mathematical simulation of thermal sintering. Modification of a Bio two-component model (of saturated porous medium) is used as the basis. Components of converted state in pores are denoted as A and B. During necking, only component B solidifies; component A is a liquid phase (water). The model is designed for describing the formation of phase boundaries and contains a set of parameters, including those with process interpretation, that enable control of phase boundary evolution. System behavior is set in time by field depending on a three-dimensional coordinate: ω_s — averaged solid phase movement velocity; ω_l — averaged

liquid phase convection velocity; z — shrinkage; c — molar concentration of component B in converted state in pores; T — temperature.

Shrinkage is defined as $z = (V - V_s - V_l)/V$, where V is the total initial system volume, V_s and V_l are current volumes of solid phase and liquid phase, respectively. The model describes non-equilibrium cold sintering under pressure: converted phase formed in pores is quickly placed in low-temperature medium, maintaining the pressure. Converted state cooling mode occurs and can be subjected to inlet pressure rise to control the neck growth process. Solid phase in pores is caused by an instability zone induced by the concentration pressure. Spinodal decomposition is implemented in this zone. c level lines are visualized in calculations, we suppose that at $c > c_{cr}$ the „liquid" (converted) phase prevails, and at $c < c_{cr}$ — the „solid" phase prevails, where c_{cr} is the threshold concentration corresponding to system instability [19]. The following system is considered as the base one:

$$\begin{bmatrix} u_t = \omega^s, \nu_t = \omega, \\ \varrho(\omega^s)_t + \varrho^l\omega_t = [\Lambda(c, a^{\pm})u_x - \alpha P]_x + \varrho g, \\ \varrho^l(\omega^s)_t + \varrho_{add}\omega_t = -D\omega - P_x + \varrho^l g + \varepsilon_M \nu_{xx}, \\ (\varrho_s + \varrho^l)_t + (\varrho^l\omega)_x + \varrho^s(\omega^s)_x = 0, \end{bmatrix} \quad (1)$$

where u is the averaged solid phase movement, ν is the averaged liquid phase movement relative to the solid phase.

System (1) is added by the equation for temperature

$$\partial_t(T + \kappa c) = D_0\partial_x^2 T, \quad (2)$$

where κ is the coefficient characterizing the internal melting heat.

Equation for the molar concentration from component B:

$$\partial_t c + \omega\partial_x f = \partial_x\left(\frac{D}{T}\partial_x c\right), \quad (3)$$

where $f(c, a^{\pm})$ is the transfer function. This is an open system — pressure is unknown.

A thermodynamically consistent expression for pressure derived from the variation (energy) analysis of non-equilibrium sintering is used as a closure equation:

$$P = P_0 + \frac{Q(1-c)^2}{qRV}\partial_c\Lambda(c, T)V_s(c_0) \times\left(\frac{V_s(c)}{V_s(c_0)} - \ln\left(\frac{V_s(c)}{V_s(c_0)}\right) - 1\right), \quad (4)$$

where P_0 is the initial pressure, Q is the heat, c is the molar component concentration, q is the heat of reaction, R is the universal gas constant, V is the total system volume, T is the temperature, $\Lambda(c, T)$ is the modulus of elasticity, V_s is the current solid phase volume, $c_(0)$ is the initial concentration of component B.

Mathematical models (1)–(4) of the initial stage (laminar process of local equilibrium approach) of three types of sintering (thermal, cold under pressure and cold vibratory) differ only in boundary conditions — inlet heating, inlet pressure rise at low temperature or inlet liquid component vibrations rise also at low temperature. Substantial difference of mathematical models appears via simulation of a labile region entrance mechanism. These are different laminar-to-turbulent transition process models that smear the resonance to release the excess energy (thermal, elastic strain under pressure or kinetic vibration of the liquid component). Different mathematical laminar-to-turbulent transition models are described by introduction of the negative Kan diffusion that induces a streak pattern in curves of variables, which is easily seen experimentally. The full-scale experiments have shown [20] that the initial necking stage is associated with the appearance of the streak pattern similar to dendritic growth during crystallization of binary alloys.

Knowing the inlet pressure $P_b(t)$ (powder pressing pressure in the presence of liquid water), equation (4) determines the molar concentration variation in pores $c_b(t) = c\,|_{x=0}$ of component B. This defines the boundary conditions for $c(x, t)$ at the input ($x = 0$):

$$c_b(t) = \frac{\frac{1}{K_0}Z(t) + \frac{c_0^0}{(1-c_0^0)}}{\left(1 + \frac{1}{K_0}Z(t) + \frac{c_0^0}{(1-c_0^0)}\right)} \geq c_0^0,$$

where $Z(t) = K_0 Y$ and

$$Y(t) = \frac{1}{\left(1 - \frac{2}{K_0^2}P_b(t)\right)}\left(\frac{2}{K_0^2}P_b(t)\left(1 + \frac{c_0^0}{(1-c_0^0)}\right) + \sqrt{\left(\frac{2}{K_0^2}P_b(t)\left(1 + \frac{c_0^0}{(1-c_0^0)}\right)\right)^2 + \frac{2}{K_0^2}P_b(t)\left(1+\frac{c_0^0}{(1-c_0^0)}\right)^2\left(1-\frac{2}{K_0^2}P_b(t)\right)}\right),$$

with initial concentration condition

$$\frac{Q}{Q+q} - c_0^0 > 0, \quad (5)$$

where $K_0 = \frac{q}{Q\left(1-y(c_0^0)\right)}$.

2. Model parameters and functions

We enlarge on the parameters and functions included in system (1)–(4). We describe the parameters and functions included in the first and second subsystems:

ϱ_s is the solid phase density, $\varrho_s = 1$ is assumed for normalization;

ϱ is the system density parameter from the Bio model, which characterizes the magnitude of the averaged kinetic energy of the solid framework of porous medium; we set $\varrho = 2.5$;

$q = m_A/m_B$, where m_A is the total weight of component A, m_B is the total weight of component B; we set $q = 0.2$;

$Q = M_A/M_B$, where M_A, M_B are atomic weights of components A and B , respectively; we set $Q = 1.4$;

m_A is the total weight of skeleton (of the embedded ceramics or polymer);

m_B is the total weight of a converted state;

c is the molar concentration of component B in the overall system, $y(c) = (qc)/(Q(1-c))$ is the mass fraction of component B in the overall system relative to the total weight of component A.

Volume occupied by the solid phase:

$$V_s = \frac{m_B(1-y(c))}{\varrho_s} = RV(1-y(c)). \tag{6}$$

Volume occupied by the liquid phase: $V_l = V - zV - V_s$, where z is the shrinkage.

We obtain an expression for the liquid phase densityϱ_l as functions c and z, i.e.

$$\varrho_l(c,z) = \varrho_s R\,\frac{q+y(c)}{1-z-R(1-y(c))},$$

where $\varrho_{add}(c,z)$ is the density of added mass from the Bio model describing the additional contribution to the kinetic energy due to a discrepancy between the microvelocity field in pores and the averaged macrovelocity.

We use the estimate

$$\varrho_{add}(c,z) = \beta\varrho_l(c,z)\,\frac{(1-z)^{\frac{1}{3}}}{(1-y(c))^{\frac{1}{3}}}.$$

We set $\beta = 0.55$; g is the effective gravity acting in porous medium, we set $g = -1/20$; $D(c,z)$ is the interfacial friction force coefficient, we also use the following estimate for this quantity:

$$D(c,z) = e^{-1/T}(1-e^{-1/T})\Gamma/(1-y(c))^{2/3}, \Gamma = 5;$$

where D is the interfacial friction coefficient (specific interfacial friction force) is estimated as $D = \Gamma_1(1-y(c))^{-2/3}((1-y(c))^{-2/3}$ is the estimate of the solid phase surface in the solid-liquid region, Γ_1 is the fitted parameter, which reflects the contribution of the surface viscosity and the averaged roughness of the solid-liquid region, as a form factor of growing dendrites. We set $\Gamma_1 = e^{-1/T}(1-e^{-1/T})\Gamma$.

In the current statement, ε_M and α are considered as constants from the Bio model. ε_M is interpreted as a measure of liquid phase flowability; joint action of ε_M and α defines the emerging porous pressure. It is assumed that α^2 is the quantity inverse to the flowability relaxation time, i.e. estimated as $\alpha \sim 10^{-3}$. For the numeric part, we set $\varepsilon_R = 20$, $\alpha = 0.04$;

$M_D(T)$ is the diffusion mobility of component B, according to [21], this quantity is estimated as $M_D(T) = D/T$;

D_0 is the coefficient characterizing thermal conductivity, for the purpose of normalization, we set $D_0 = 1$.

3. Model of cold sintering under pressure (local equilibrium approximation)

We proceed to mathematical simulation of the laminar mode of the sintering process. We assume that in model (1)–(4), the normal modulus of elasticity is:

$$\Lambda(c,a^+,a^-) = \Lambda_0(Ac - B), \quad \Lambda_0 = \text{const} > 0, \tag{7}$$

where $A = a^+ + a^-$, $a^\pm = \text{const} \in (0,1)$, $a^+ > a^-$, $B = a^+a^-$.

Then for the modulus of elasticity

$$\Lambda(c,a^\pm) = \Lambda_0(a^+(c-a^-) + ca^-) > 0,$$

$$\partial_c\Lambda(c,T) = A > 0. \tag{8}$$

According to (5), if

$$a^- < c < a^+ < \frac{Q}{(Q+q)}. \tag{9}$$

We require that, for the initial concentration, the condition of entrance in the labial region for the free energy potential of the laminar-to-turbulent transition is met: $a^- < c_0 < a^+ < \frac{Q}{Q+q}$.

Transfer function: $f(c,a^-) = -\frac{1}{2}(c - \frac{1}{2}A)^2$.

Model parameters and functions are described above.

Hyperbolicity conditions

$$\Lambda > 0,\ \varepsilon_M > 0,\ \varrho\varrho_{add} - (\varrho^l)^2 > 0,\ \varrho - \varrho^l > 0.$$

Two elastic waves and two surface waves (counterparts of the Stonely waves in the Bio model). $\partial_c\Lambda = a^+ + a^- > 0$ is met and $(P - P_0) \geq 0$, if

$$a^+ < \frac{Q}{(q+Q)}. \tag{10}$$

4. Initial-boundary conditions of the cold sintering process in the local equilibrium approximation

We solve a mixed problem with initial-boundary conditions. All processes in the model are considered on a one-dimensional interval [0,1], At the initial time, at the input boundary $x = 0$, increased pressure and decreased initial temperature are set.

So, we describe the initial conditions

$$u(0,x) = v(0,x) = \omega_s(0,x) = \omega(0,x) = 0;$$

$$z(0,x) = 0; \quad T(0,x) = \text{const}.$$

Initial conditions for the concentration of:

— one neck

$$c(0,x) = c_{\max}, \quad 0 < x < 1/3$$

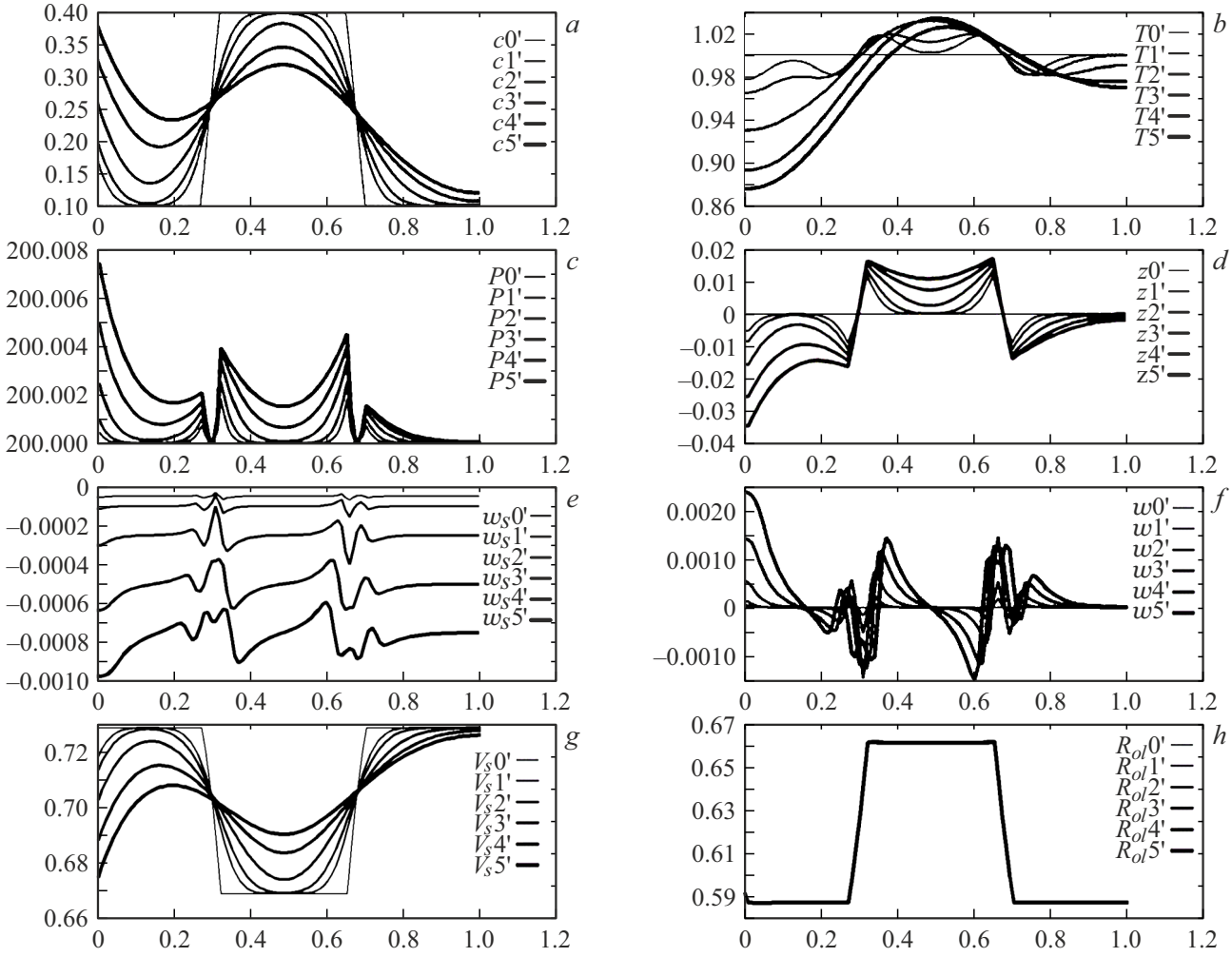

Figure 1. Time cross-section curves at $t = 0$; 0.001; 0.002; 0.005; 0.01; 0.015: *a* — molar concentration from component *B* in pore; *b* — temperature *T*; *c* — pressure *P*; *d* — shrinkage *Z*; *e* — averaged solid phase movement velocity W_s; *f* — averaged liquid phase movement velocity relative to the solid phase *W*; *g* — solid phase volume V_s; *h* — liquid phase density ϱ_l.

and

$$2/3 < x < 1; \quad c(0, x) = c_{\min}, \quad \frac{1}{3} < x < 23;$$

— two necks

$$c(0, x) = c_{\max}, \ 0 < x < 0.2; \ 0.4 < x < 0.6; \ 0.8 < x < 1,$$

$$c(0, x) = c_{\min}, \quad 0.2 < x < 0.4; \quad 0.6 < x < 0.8.$$

Then we describe the boundary conditions

$$\partial_x \omega(t, 0) = \partial_x \omega_s(t, 0) = \partial_x \omega(t, 1) = \partial_x \omega_s(t, 1) = 0, \tag{11}$$

$$\partial_x c(t, 1) = 0,$$

$$\partial_x z(t, 0) = \partial_x z(t, 1) = \partial_x T(t, 0) = \partial_x T(t, 1) = 0,$$

$$c\,|_{x=0} = c_b(t)\ , \ c_b(0) = c^0\,|_{x=0}\ ; \quad P_b(t) = P_0^0 + \beta t.$$

We simulate cold sintering under pressure $P_b(t)$, which we increase with time.

5. Numerical experiment of local equilibrium approximation

One neck. Example 1 (Figure 1). $c_{\max} = 0.6$, $c_{\min} = 0.1$, $\kappa = 1$, $P_0 = 150$, $T_0 = 1$, $\beta = 0.5$. Cross-sections $t = 0$; 0.001; 0.002; 0.005; 0.01; 0.015; $a^+ = 7/8 - 0.01$; $a^- = 0.2$. This set of parameters can be called the base set, it simulates typical properties of the initial cold sintering mode under pressure in the case of necking simulation.

Clearly pronounced streaking can be seen here (especially on the temperature curve). There is a local temperature rise in the labial region. Transition into a purely diffusion process can be seen on the temperature curve (temperature curve in the solid phase becomes convex). Converted state grows under pressure in the solid phase region (molar concentration of component *B* grows).

The solid phase volume grows in the pore (neck is generated). These are basic qualitative properties of numerical experiments shown below.

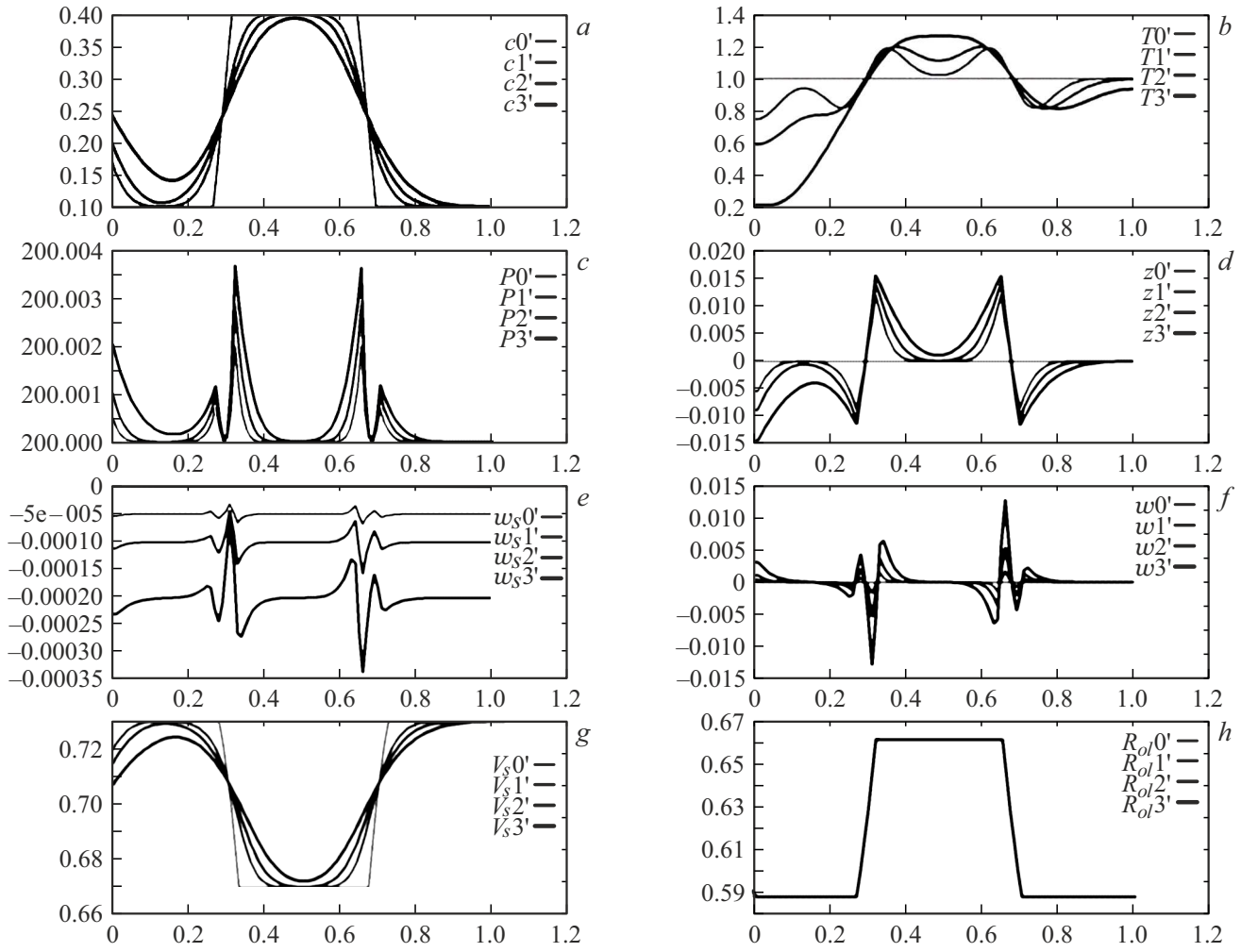

Figure 2. Time cross-section curves at $t = 0$; 0.001; 0.002; 0.005; 0.01; 0.015: *a* — molar concentration from component *B* in pore; *b* — temperature *T*; *c* — pressure *P*; *d* — shrinkage *Z*; *e* — averaged solid phase movement velocity W_s; *f* — averaged liquid phase movement velocity relative to the solid phase *W*; *g* — solid phase volume V_s; *h* — liquid phase density ϱ_l.

Preliminary numerical analysis has shown the presence of a strict upper-bound estimate for $c_{\max}$, which has determined the choice for the numerical experiment $c_{\max} = 0.6$. This suggests that a very high concentration of neutral component *A* (water) in pores is required.

Example 2 (Figure 2). $c_{\max} = 0.6$, $c_{\min} = 0.1$, $\kappa = 10$, $P_0 = 150$, $T_0 = 1$, $\beta = 0.5$. Cross-sections $t = 0$; 0.001; 0.002; 0.005; 0.01; 0.015; $a^+ = 7/8 - 0.01$; $a^- = 0.2$. From comparison of the first two numerical experiments it can be seen that the internal melting heat k is a critical parameter. Increase in k brings the resonance closer ($T = 0$) and breaks the streaky pattern of the temperature curve, so the temperature curve tends to a convex classical diffusion process curve. Considerable increase in k leads to fast resonance breakdown ($T = 0$).

Two necks. Example 1 (Figure 3). $\kappa = 2.5$, $P_0 = 150$, $\beta = 3$. Cross-sections $t = 0$; 0.0005; 0.005; 0.01; 0.015; $a^+ = 7/8 - 0.01$; $a^- = 0.2$. This set of parameters can be called the base one, it simulates typical properties of the initial cold sintering mode under pressure and for simulation of generation of two necks.

Clearly pronounced streaking is particularly apparent on the temperature curve. There is a local temperature rise in the labial region. Transition into a purely diffusion process can be seen on the temperature curve (temperature curve in the solid phase becomes convex). Converted state grows under pressure in the solid phase region (molar concentration of component B grows). Solid phase volume in pores increases.

Example 2 (Figure 4). $c_{\max} = 0.6$, $c_{\min} = 0.1$, $\kappa = 10$, $P_0 = 150$, $T_0 = 1$, $\beta = 0.5$. Cross-sections $t = 0$; 0.001; 0.002; 0.005; 0.01; 0.015; $a^+ = 7/8 - 0.01$; $a^- = 0.2$. Here, increase in k also brings the resonance closer ($T = 0$).

Conclusion

Clearly pronounced streaking is apparent at the initial sintering stage (particularly on the temperature curve).

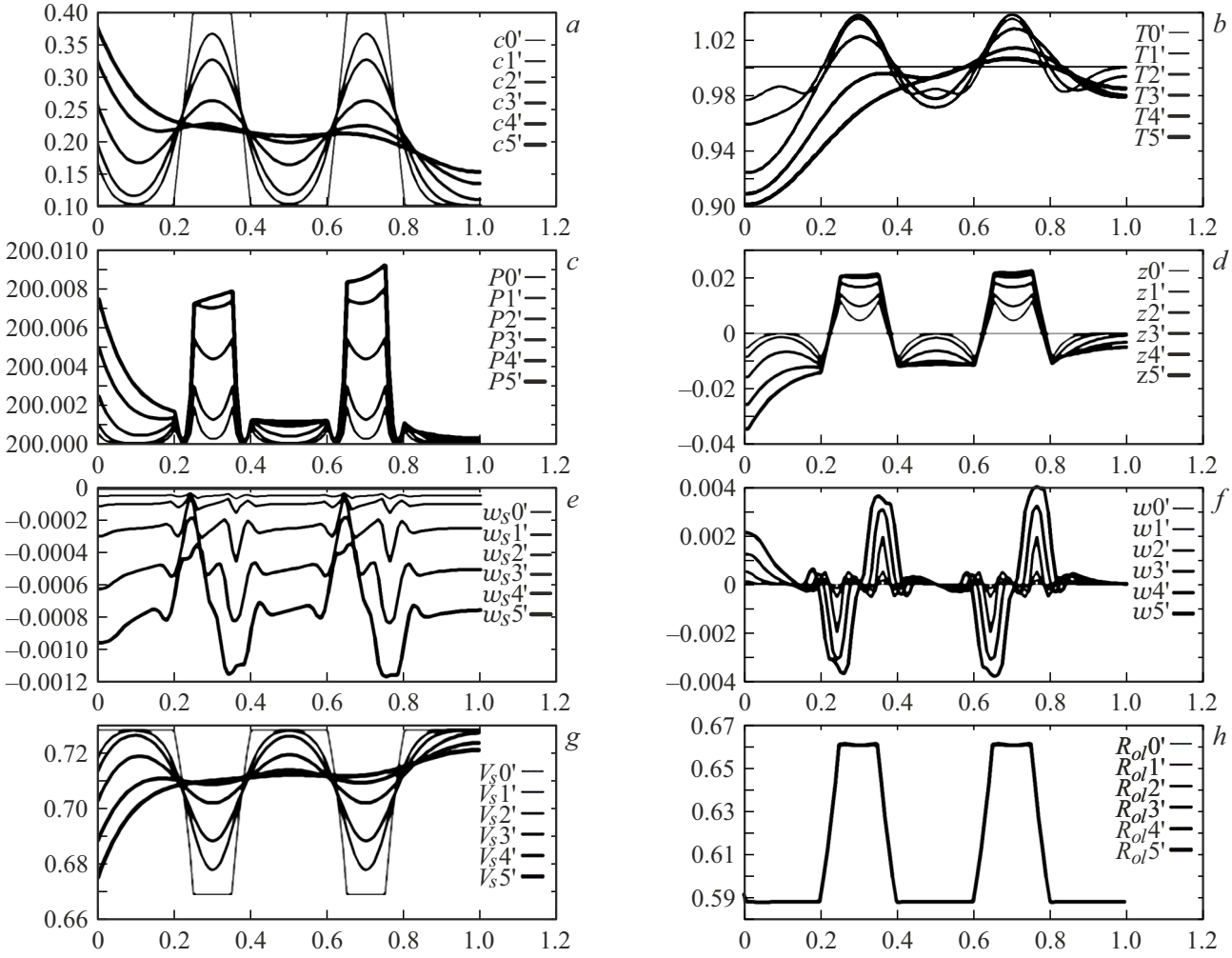

Figure 3. Time cross-section curves at $t = 0$; 0.0005; 0.005; 0.01; 0.015: *a* — molar concentration from component *B* in pore; *b* — temperature *T*; *c* — pressure *P*; *d* — shrinkage *Z*; *e* — averaged solid phase movement velocity W_s; *f* — averaged liquid phase movement velocity relative to the solid phase *W*; *g* — solid phase volume V_s; *h* — liquid phase density ϱ_l.

There is a local temperature rise in the labial region. Transition into a purely diffusion process can be seen on the temperature curve (temperature curve in the solid phase becomes convex). Converted state grows under pressure in the solid phase region (molar concentration of component *B* grows). The solid phase volume grows in the pore (a neck is generated).

Sintering process turbulization is a process with energy, excess of which in the laminar stage leads to the Rauschenbach resonance. Resonance can be avoided by abrupt transition from a local equilibrium manifold to the laminar-to-turbulent transition, which will smear the resonance by transition to a converted state and drastically increase the streaking (diffusion separation) existence time. In the streaking existence region, according to the full-scale experiment, initial neck growth occurs at a rate, which is by an order of magnitude higher than the diffusion one.

Outside the labial region, the temperature decreases. The process is quickly stabilized (depending on the internal melting heat κ) to the classical volume diffusion (the temperature curve stabilizes to the convex function curve). Internal melting heat κ is a critical parameter. As it increases, acceleration of stabilization towards the volume diffusion and resonance approach occur simultaneously ($T = 0$), which corresponds to the Rauschenbach description of vibration pressure.

As a result, the initial cold sintering stage constitutes a non-equilibrium phase transition; its mechanism is defined by diffusion separation.

Funding

The study was performed according to Agreement No 075-15-2024-527 dated April 23, 2024, On the Provision of a Grant from the Federal Budget for Major Research Projects in Priority Research and Development Areas

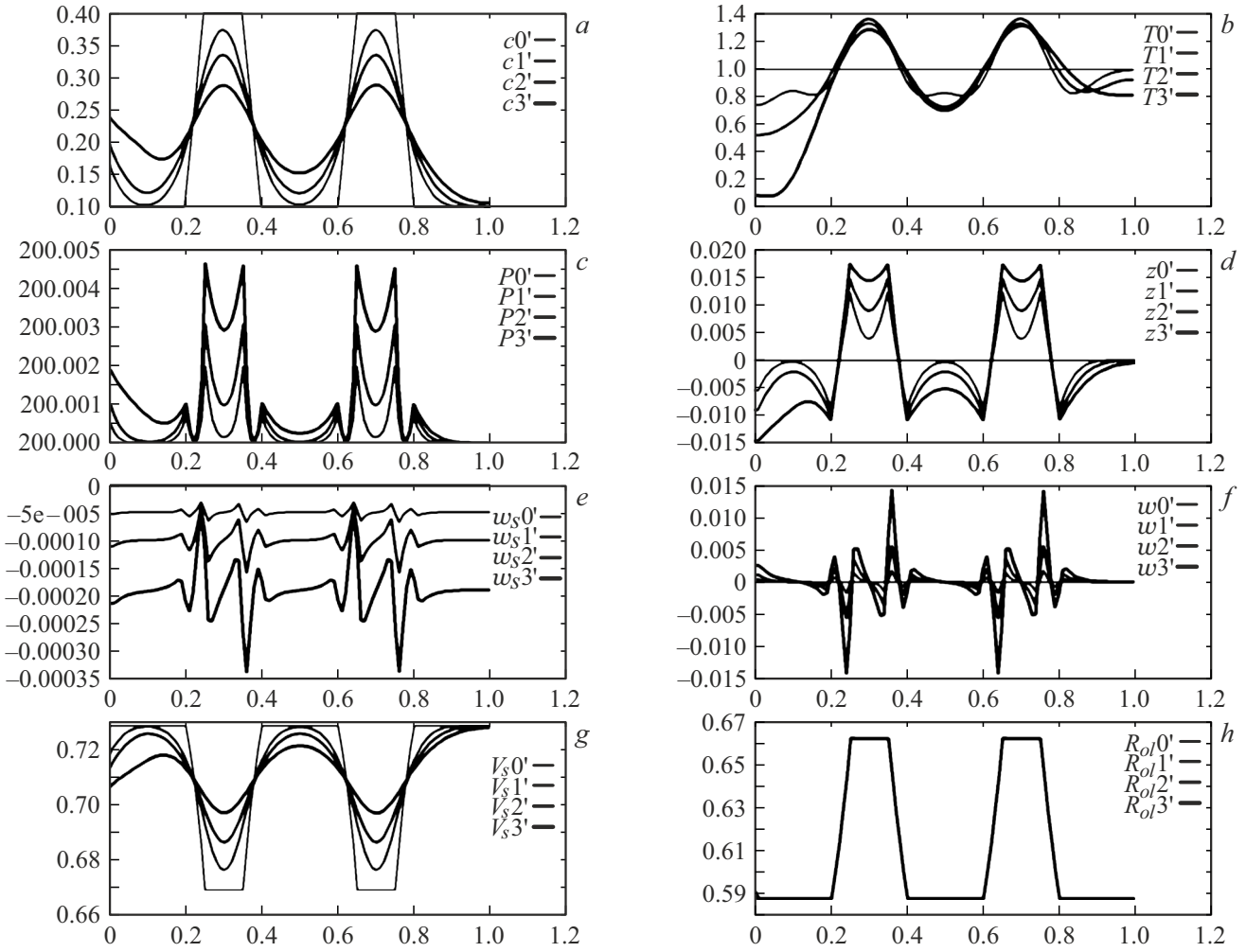

Figure 4. Time cross-section curves at $t = 0$; 0.001; 0.002; 0.005; 0.01; 0.015: *a* — molar concentration from component *B* in pore; *b* — temperature *T*; *c* — pressure *P*; *d* — shrinkage *Z*; *e* — averaged solid phase movement velocity W_s; *f* — averaged liquid phase movement velocity relative to the solid phase *W*; *g* — solid phase volume V_s; *h* — liquid phase density ϱ_l.

Author contributions

All authors have made equal contributions to the research work.

Conflict of interest

The authors declare no conflict of interest.

References

[1] M. Biesuz, G. Taveri, A.I. Duff, E. Olevsky, D. Zhu, C. Hu, S. Grasso. Adv. Appl. Ceram., **119** (2), 75 (2020). DOI: 10.1080/17436753.2019.1692173

[2] J. Guo, H. Guo, A.L. Baker, M.T. Lanagan. Angewandte Chemie. Int. Ed., **55**, 11457 (2016). DOI: 10.1002/anie.201605443.

[3] C.A. Randall, J. Guo, A. Baker, M. Lanagan, H. Guo. *Cold sintering ceramics and composites* (US20170088471A1, 2017)

[4] J. Guo, S.S. Berbano, H. Guo, A.L. Baker, M.T. Lanagan, C.A. Randall. Adv. Functional Mater., **26**, 7115 (2016). DOI: 10.1002/adfm.201602489

[5] S. Funahashi, H. Guo, J. Guo, A.L. Baker, K. Wang, K. Shiratsuyu, C.A. Randall. J. American Ceramic Society, **100** (8), 3488 (2017). DOI: 10.1111/jace.14852

[6] F. Bouville, A.R. Studart. Nat. Commun., **8** (1), 14655 (2017). DOI: 10.1038/ncomms14655

[7] S. Funahashi, J. Guo, H. Guo, K. Wang. J. American Ceramic Society, **100**, 546 (2017). DOI: 10.1111/jace.14617

[8] J. Gonzalez-Julian, K. Neuhaus, M. Bernemann, J.G.P. da Silva. A.M. Laptev, M. Bram, O. Guillon. Acta Mater., **144**, 116 (2018). DOI: 10.1016/j.actamat.2017.10.055

[9] J.A. Liu, C.H. Li, J.J. Shan, J.-M. Wu, R.-F. Gui, Yu. Shi. Mater. Sci. Semicond. Process., **84**, 17 (2018). DOI: 10.1016/j.mssp.2018.04.030.21

[10] V. Medri, F. Servadei, R. Bendoni, A.N. Murri, A. Vaccari, E. Landi. J. Europ. Ceramic Society, **39** (7), 2453 (2019). DOI: 10.1016/j.jeurceramsoc.2019.02.047

[11] H. Guo, J. Guo, A. Baker, C.A. Randall. ACS Appl. Mater. Interfaces, **8** (32), 20909 (2016). DOI: 10.1021/acsami.6b07481

[12] H. Guo, A. Baker, J. Guo, C.A. Randall. J. American Ceramic Society, **99** (11), 3489 (2016). DOI: 10.1111/jace.14554
[13] J.H. Seo, J. Guo, H. Guo, K. Verlinde, D.S.B. Heidary, R. Rajagopalan, C.A. Randall. Ceramics Intern., **43** (17), 15370 (2017). DOI: 10.1016/j.ceramint.2017.08.077
[14] A. Ndayishimiye, S. Buf, M. Dourges, A. Largeteau, M. Prakasam, St. Mornet, O. Kaman, O. Kaman, J. Zdeněk, J. Hejtmanek, G. Goglio. Scripta Mater., **148**, 15 (2018). DOI: 10. 1016/j.scriptamat.2018.01.013
[15] I.J. Induja, M.T. Sebastian. Mater. Lett., **211**, 55 (2018). DOI: 10.1016/j.matlet.2017.09.083.
[16] A. Jiang, D. Ke, L. Xu, Q. Xu, J. Li, J. Wei, Ch. Hu, S. Grasso. J. Materiomics, **5** (3), 496 (2019). DOI: 10.1016/j.jmat.2019.02.009
[17] S. Grasso, M. Biesuz, L. Zoli, G. Taveri, A.I. Duff, D. Ke, A. Jiang, M.J. Reece. Advances Appl. Ceramics, **119** (3), 115 (2020). DOI: 10.1080/17436753.2019.1706825
[18] G. Taveri, S. Grasso, F. Gucci, J. Toušek, I. Dlouhy. Advanced Functional Mater., **28** (48), 1805794 (2018). DOI: 10.1002/adfm.201805794
[19] E.V. Radkevich, O.A. Vasilieva, M.I. Sidorov. DAN, **489** (6), 545 (2019) (in Russian). DOI: 10.31857/S0869-56524896545-551
[20] E.V. Radkevich, O.A. Vasilieva, N.N. Yakovlev i dr. *Matematicheskoe modelirovanie detonatsionnogo goreniya* (Eko-Press, M., 2024), 200 s. (in Russian)
[21] W. Dreyer, B. Wagner. Interfaces Free Boundaries, **7** (2), 199 (2005). DOI: 10.4171/IFB/121

Translated by E.Ilyinskaya